crystals

MDPI

Article

Finding Crystal Orientations in Uniplanar Textures

Josef Simbrunner [1,*], Fabian Gasser [2], Sanjay John [2], Ingo Salzmann [3,4,5] and Roland Resel [2]

[1] Division of Neuroradiology, Vascular and Interventional Radiology, Medical University Graz, Auenbruggerplatz 9, 8036 Graz, Austria
[2] Institute of Solid State Physics, Graz University of Technology, Petersgasse 16, 8010 Graz, Austria; fabian.gasser@tugraz.at (F.G.); sanjayjohn@tugraz.at (S.J.); roland.resel@tugraz.at (R.R.)
[3] Department of Physics, Concordia University, Montreal, QC H4B 1R6, Canada; ingo.salzmann@concordia.ca
[4] Department of Chemistry and Biochemistry, Concordia University, Montreal, QC H4B 1R6, Canada
[5] Centre for Research in Molecular Modeling (CERMM), Centre for NanoScience Research (CeNSR), Concordia University, Montreal, QC H4B 1R6, Canada
* Correspondence: josef.simbrunner@medunigraz.at

Abstract: The crystallization of molecular materials on isotropic substrates typically results in a so-called fiber or uniplanar texture that comprises crystallites that share a common fiber axis perpendicular to the substrate surface, but that are azimuthally randomly oriented. The crystallographic characterization of such films is commonly performed by grazing-incidence X-ray diffraction. Thereby, two-dimensional reciprocal space maps are obtained that incorporate the in-plane component q_{xy} and the out-of-plane component q_z for each diffraction peak. The exact position of each diffraction peak depends on the crystallographic lattice and on the orientation of the unit cell relative to the substrate surface. The unit cell orientation can be characterized either by two rotation angles or by the Miller indices of the crystallographic plane (contact plane) parallel to the substrate surface. Equations are derived that allow the calculation of these orientation parameters and describe the relations between them. Depending on the crystallographic system of the underlying unit cell and its contact plane, manifold possible orientations may exist due to the multiplicity of planes contributing to the same reflections. Examples based on molecular crystals of pentacenequinone, diindenoperylene, and binaphthalene are discussed, which are illustrative examples comprising triclinic, monoclinic, and tetragonal unit cells having two, four, and sixteen possible crystal orientations, respectively.

Keywords: uniplanar textures; grazing-incidence X-ray diffraction; orientation matrix; contact plane

check for updates

Academic Editor: Benoit Heinrich

Received: 3 April 2025
Revised: 2 May 2025
Accepted: 5 May 2025
Published: 8 May 2025

Citation: Simbrunner, J.; Gasser, F.; John, S.; Salzmann, I.; Resel, R. Finding Crystal Orientations in Uniplanar Textures. *Crystals* **2025**, *15*, 443. https://doi.org/10.3390/cryst15050443

Copyright: © 2025 by the authors. Licensee MDPI, Basel, Switzerland. This article is an open access article distributed under the terms and conditions of the Creative Commons Attribution (CC BY) license (https://creativecommons.org/licenses/by/4.0/).

1. Introduction

In the presence of a substrate during crystal growth, crystallites in thin films can adopt a preferred orientation (texture) [1]. On isotropic substrates, the crystallization of molecular materials typically results in so-called fiber or uniplanar textured films that comprise crystallites that share a common fiber axis perpendicular to the substrate surface, but that are azimuthally randomly oriented [2]. In the case of thin films formed by conjugated organic molecules, their growth occurs typically in crystal systems of low symmetry (in most cases, monoclinic and triclinic) with a strong tendency to polymorphism, which makes crystal structure determination an important task [3]. Additionally, unknown polymorphs of organic materials are often observed within thin films only, and therefore cannot be determined independently via traditional methods such as single-crystal diffraction.

Due to its surface sensitivity, grazing-incidence X-ray diffraction (GIXD) is particularly suited for investigations of the crystalline properties of thin films [4,5]. The surface sensitivity of GIXD is due to the angle of incidence of the primary beam relative to the sample surface (α_i) being chosen close to the critical angle of total external reflection. The primary X-ray beam described by the wave vector $\mathbf{k_0}$ and a given scattered beam $\mathbf{k}$ together determine the scattering vector $\mathbf{q} = \mathbf{k} - \mathbf{k_0}$. According to the Laue equation, diffraction occurs if $\mathbf{q}$ is equal to a reciprocal lattice vector $\mathbf{g}$. For organic crystallites in fiber-textured films, the reciprocal lattice points lie on concentric circles. Keeping the sample fixed in space, a GIXD experiment then equals a cut through the 3D reciprocal space, roughly perpendicular to the rings of reciprocal lattice points. Thus, a corresponding two-dimensional reciprocal space map is obtained that comprises the in-plane component q_{xy} and the out-of-plane component q_z for each diffraction peak.

A key direction in reciprocal space is the z-direction at $q_{xy} = 0$, which reveals the orientation of crystals relative to the substrate surface. In the important case of crystalline fiber-textured films, it defines the crystallographic plane (the so-called contact or texture plane) of the thin film crystallites that is parallel to the substrate surface. In the GIXD geometry, however, this specific z-direction is inaccessible in reciprocal space. To experimentally assess scattering in this direction, one must therefore resort to specular X-ray diffraction, where the incidence angle of the primary beam and the exit angle of the scattered X-ray beam are equal. This results in a scattering vector $\mathbf{q}$ always oriented perpendicular to the substrate surface, and the scattering vector then exclusively has a q_z component (with $q_{xy} = 0$). In the following, a diffraction peak observed via specular X-ray diffraction is denoted as q_{spec}. The presence of a specular diffraction peak indicates that the substrate surface corresponds to a crystallographic plane of the underlying unit cell of the investigated molecule, which can be specified by the Miller indices, i.e., the integers u, v, and w. Incorporating information acquired by specular diffraction into the analysis, indexing GIXD patterns can be significantly facilitated, as equations can be derived in which the real lattice parameters and the number of unknown integer parameters (Laue and Miller indices) are reduced [6,7].

In anisotropic crystals, the optoelectronic properties may vary in certain spatial directions. Therefore, characterizing the orientation of crystallites adsorbed on solid substrates, i.e., their texture, is of key importance for functional structures [8–14]. Determining the orientation of the unit cell is an integral constituent of indexing static GIXD patterns. In the case of rotated unit cells, i.e., if the contact plane is different from (001), indexing becomes a demanding task, which, in most cases, is solved by trial and error. Even in our previously developed systematic approach, however, determining the orientation parameters was given a secondary role. In the present work, we now focus on determining the orientation parameters in fiber-textured films with known lattice parameters, introducing a systematic algorithm. To this end, thin films of crystallites that belong to three different crystal systems (triclinic, monoclinic, and tetragonal) with contact planes that possess diverse Miller indices are exemplarily analyzed.

2. Materials and Methods

2.1. Investigated Materials

Thin films of 6,13-pentacenequinone (P2O, $C_{22}H_{12}O_2$) and diindenoperylene (DIP, $C_{32}H_{16}$) were grown on a freshly cleaved highly oriented pyrolytic graphite substrate (HOPG, ZYA grade) by physical vapor deposition under high-vacuum conditions (base pressure $< 5 \times 10^{-6}$ Pa). In both cases, the final nominal film thickness was 30 nm, as determined by a quartz crystal microbalance. The films were characterized at beamline W1 at the synchrotron radiation facility DORIS (HASYLAB, Hamburg, Germany). GIXD

experiments were performed following specular X-ray diffraction using a wavelength of 1.1796 Å for the primary X-ray beam, a goniometer in pseudo 2 + 2 geometry, and a one-dimensional detector (MYTHEN, Dectris, Baden, Switzerland) with primary and secondary slits; no sample realignment was required between the two experimental techniques. For the GIXD experiments, the incident angle of the primary beam was set to $\alpha_i = 0.13°$. The in-plane scattering angle θ_f was varied between 3° and 40° in steps of 0.05°, where for every step, an out-of-plane scattering range of $\Delta\alpha_f = 3.5°$ was recorded. In total, seven scans along θ_f were performed so that the complete covered angular range of α_f was 0° to 24.5°. More detailed information can be found in our previous publications [6,7].

Thin films of 1,1′-binaphthalene (BNP, $C_{20}H_{14}$) were prepared by spin coating through static dispensing from a 70 g/L dichloromethane solution using a spin velocity of 6000 rpm. The used silicon substrates were atomically flat and native oxide layer terminated. Prior to use, the substrates were cleaned with acetone and isopropanol and sonicated in an acetone bath. GIXD experiments were performed at the beamline XRD1, synchrotron Elettra (Trieste), using a wavelength of 1.4 Å and an incidence angle of $\alpha_i = 1.0°$. The diffracted signal was recorded on a static two-dimensional detector (Pilatus 2M, Dectris) positioned at a nominal sample–detector distance of 20 cm. To achieve better statistics, diffraction signals were integrated over a full sample rotation around the surface normal. Further details are provided in a separate publication [15].

2.2. Theoretical Methods

The reciprocal lattice vector $\mathbf{g_{001}}$ with its Laue indices h, k, and l can be represented by the equation

$$\mathbf{g} = \boldsymbol{R}(u, v, w)\boldsymbol{A}^* \begin{pmatrix} h \\ k \\ l \end{pmatrix} = \boldsymbol{R}(\psi, \Phi)\boldsymbol{A}^* \begin{pmatrix} h \\ k \\ l \end{pmatrix}, \tag{1}$$

where the matrix $\boldsymbol{A}^*$ contains the vectors of the reciprocal lattice and $\boldsymbol{R}$ is a rotation matrix, which can be either characterized by the Miller indices of the contact plane (uvw) or by the angles ψ and Φ that define the orientation of the rotation axis and the rotation angle, respectively. A comprehensive mathematical treatise can be found in our previous work [6] and is summarized in Appendix A. In the unrotated case, i.e., for the contact plane (001), $\boldsymbol{R}$ is the unit matrix. Generally, Φ and ψ can take a continuous spectrum of values, whereas, in the case of a contact plane, they are specified by integers, i.e., its Miller indices. Note also that any rotation of the reciprocal lattice vectors corresponds to an identical rotation of the lattice vectors in the real space. When the Laue condition $\mathbf{q} = \mathbf{g}$ is fulfilled, diffraction can be observed.

Using the notation with the Miller indices, the explicit expressions for the length of the reciprocal vector $g_{xyz} = \sqrt{g_{xy}^2 + g_z^2}$ and for g_z can be written as follows:

$$g_{xyz} = \sqrt{h^2a^{*2} + k^2b^{*2} + l^2c^{*2} + 2hka^*b^*\cos\gamma^* + 2hla^*c^*\cos\beta^* + 2klb^*c^*\cos\alpha^*}, \tag{2}$$

$$\begin{aligned} g_z = [&ha^*(ua^* + vb^*\cos\gamma^* + wc^*\cos\beta^*) + kb^*(vb^* + ua^*\cos\gamma^* + wc^*\cos\alpha^*) \\ &+ lc^*(wc^* + ua^*\cos\beta^* + vc^*\cos\alpha^*)]/g_{spec}. \end{aligned} \tag{3}$$

For convenience, in Equations (2) and (3), the direct and reciprocal lattice parameters are used (cf., Appendix A); g_{spec} is the length of the specular diffraction peak. Note that q_{xyz} (cf. Equation (2)) is orientation-independent. If the lattice parameters are known, using this expression, indexing, i.e., assigning the Laue indices, can be conveniently performed. Furthermore, it follows that it is algebraically not possible to determine Φ and ψ from one given pair (q_{xy}, q_z) of an observed peak.

Using the notation with Φ and ψ, Equation (3) can be written alternatively [16] as follows:

$$g_z = ha^*[\cos\Phi\cos\beta^* + \sin\Phi\sin\beta^*\cos(\gamma-\psi)] + kb^*(\cos\Phi\cos\alpha^* - \sin\Phi\sin\alpha^*\cos\psi) + lc^*\cos\Phi. \quad (4)$$

Obviously, Equations (3) and (4) can be expressed in the common form

$$g_z = ha^*f_1 + kb^*f_2 + lc^*f_3. \quad (5)$$

Using the out-of-plane component of three reflections, the coefficient f_i can be easily obtained if the associated equations are linearly independent. In further consequence, from Equation (4), the following expressions can be derived:

$$\cos\Phi = f_3, \quad (6)$$

$$\cos\psi = \frac{\cos\Phi\cos\alpha^* - f_2}{\sin\Phi\sin\alpha^*}, \quad (7)$$

and

$$\cos(\gamma-\psi) = \frac{f_1 - \cos\Phi\cos\beta^*}{\sin\Phi\sin\beta^*}. \quad (8)$$

Combining Equations (6) to (8), the following equation can be obtained:

$$\tan\psi = -\frac{\sin\alpha}{\sin\beta\sin\gamma}\frac{f_1 - f_3\cos\beta^*}{f_2 - f_3\cos\alpha^*} - \cot\gamma. \quad (9)$$

In the unrotated case, f_3 = 1. Equations (7) and (9) determine the quadrant of ψ. For more than three reflections, Equation (5) is overdetermined and the solution can be analytically optimized (see Appendix B).

If the notation with the Miller indices u, v, and w is used, the following relation can be derived (see Appendix A):

$$v = u\frac{b}{a}\frac{\sin(\psi-\gamma)}{\sin\psi}. \quad (10)$$

Using Equations (3), (4), and (10), after some algebraic work, the following expressions can be obtained:

$$g_{spec} = \frac{u}{a}\frac{2\pi}{\sin\Phi\sin\psi}, \quad (11)$$

and

$$w = u\frac{c}{a}\left[\sin\beta\left(\sin\alpha^*\frac{\cot\Phi}{\sin\psi} + \cos\alpha^*\cot\psi\right) + \cos\beta\right]. \quad (12)$$

Note that algebraically, u can be freely chosen. As the Miller indices v and w must be integers, its value is determined so that the smallest common divisor of u, v, and w is one. If specular diffraction has been performed, u is determined by Equation (11). Rotating GIXD experiments, where all vector components of the diffraction peaks are obtained and therefore the lattice vectors of the unit cell can be determined, have shown that in the investigated thin films for the same type of molecular crystal, contact planes characterized by Miller indices u, v, and w coexist with those with -u, -v, and -w, which results in a mirror symmetry being equally present [17,18]. In static GIXD experiments, it cannot be differentiated between the contact planes (uvw) and $(\overline{uvw})$, as the corresponding diffraction peaks $(q_{xy}, q_z)_{(uvw)}$ and $(q_{xy}, q_z)_{(\overline{uvw})}$ overlap.

Equation (3) can be also be written in the following way:

$$\begin{aligned} g_z = [&ha^*(u_qa^* + v_qb^*\cos\gamma^* + w_qc^*\cos\beta^*) + kb^*(v_qb^* + u_qa^*\cos\gamma^* + w_qc^*\cos\alpha^*) \\ &+ lc^*(w_qc^* + u_qa^*\cos\beta^* + v_qc^*\cos\alpha^*)], \end{aligned} \quad (13)$$

where $u_q = \frac{u}{g_{spec}}$, $v_q = \frac{v}{g_{spec}}$, and $w_q = \frac{w}{g_{spec}}$. The parameters u_q, v_q, and w_q can be alternatively chosen as real rotation parameters if no specular scan is available or if it does not show a detectable peak corresponding to the contact plane [19]. Combining Equations (5) and (13), the following expression can be derived:

$$\begin{pmatrix} a^* & b^* \cos\gamma^* & c^* \cos\beta^* \\ a^* \cos\gamma^* & b^* & c^* \cos\alpha^* \\ a^* \cos\beta^* & b^* \cos\alpha^* & c^* \end{pmatrix} \begin{pmatrix} u_q \\ v_q \\ w_q \end{pmatrix} = \begin{pmatrix} f_1 \\ f_2 \\ f_3 \end{pmatrix}. \quad (14)$$

From Equation (14), u_q, v_q, and w_q can be easily obtained. By building the ratios of these factors, the Miller indices of the contact plane may be found. The expressions that lead from these parameters to the angles Φ and ψ can be found in Appendix C, together with reduced expressions for the rotation parameters in monoclinic or orthorhombic crystal systems.

3. Results and Discussion

In the following paragraphs, we want to apply our theoretical results to various illustrative examples representing several orders of crystallographic symmetry. Assigning the Laue indices to the diffraction peaks is the prerequisite for determining the orientation of the unit cell. Substrate peaks do not play a role.

3.1. Pentacenequinone (P2O) on HOPG—Triclinic

Indexing was performed using our algorithm incorporating the information of the specular diffraction peak indicating that a crystallographic contact plane exists [6]. In Figure 1a, the GIXD pattern of a P2O thin film adsorbed on HOPG is shown.

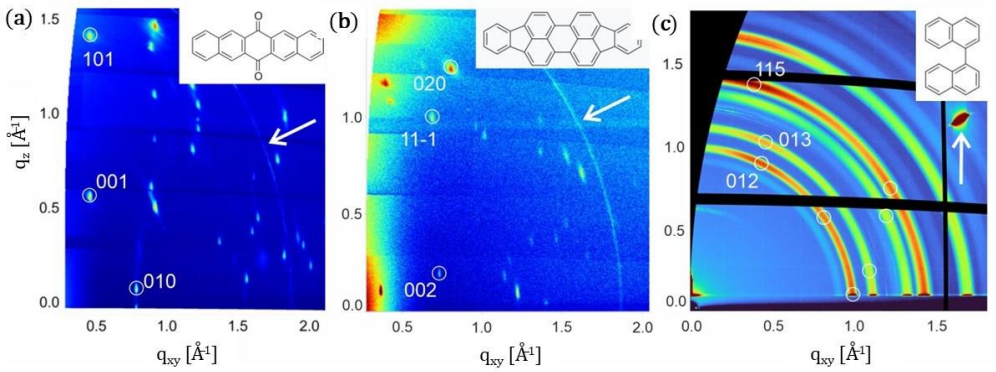


Figure 1. GIXD patterns of (**a**) pentacenequinone (P2O), (**b**) diindenoperylene (DIP), and (**c**) binaphthalene crystals. For clarity, Laue indices are given only for selected Bragg peaks; positions were calculated for the contact planes (102) in P2O (**a**), (121) in DIP (**b**), and (217) in BNP (**c**). The arrows indicate diffraction features of the substrate. The chemical structures of the molecules are given as insets.

The 74 most intense reflections of the GIXD map were included in the analysis; the obtained lattice parameters are given in Table 1. The low mosaicity allows an unambiguous assignment of the peak positions q_{xy} and q_z. Using these lattice parameters, the out-of-plane components, and the Laue indices associated with the 74 reflections, the rotation angles Φ and ψ were calculated. The obtained values and their errors are given in Table 2.

Table 1. Lattice parameters of P2O/HOPG, DIP/HOPG, and BNP/Si. If available, the length of the specular diffraction peak (q_{spec}) is also listed.

a [Å]	b [Å]	c [Å]	α [°]	β [°]	γ [°]	Vol [Å^3]	q_{spec} [Å^{-1}]
P2O/HOPG [6]							
5.067 (16)	8.064 (39)	8.882 (28)	91.64 (27)	93.34 (41)	94.01 (28)	361	1.946
DIP/HOPG [7]							
7.149 (50)	8.465 (41)	16.62 (36)	90	93.14 (93)	90	1004.5	1.776
BNP/Si [20]							
7.181	7.181	27.681	90	90	90	1427.4	not available

Table 2. Determined orientation parameters of P2O/HOPG, DIP/HOPG, and BNP/Si obtained in GIXD experiments.

Φ [°]	ψ [°]	u_q	v_q	w_q	contact plane
P2O/HOPG					
39.87 (37)	94.42 (54)	0.5151 (38)	0.0000 (50)	1.0279 (40)	(102)
140.13 (37)	274.42 (54)	−0.5151 (38)		−1.0279 (40)	$(\bar{1}0\bar{2})$
DIP/HOPG					
76.27 (41)	30.87 (20)	0.5677 (46)	−1.1237 (42)	0.5545 (93)	$(1\bar{2}1)$
	149.13 (20)		1.1237 (42)		(121)
103.73 (41)	210.87 (20)	−0.5677 (46)		−0.5545 (93)	$(\bar{1}2\bar{1})$
	329.13 (20)		−1.1237 (42)		$(\bar{1}\bar{2}1)$
BNP/Si					
51.2 (16)	27.1 (12)	0.408 (21)	−0.794 (19)	2.762 (21)	$(1\bar{2}7)$
	152.9 (12)		0.794 (19)		(127)
	207.1 (12)	−0.408 (21)			$(\bar{1}27)$
	332.9 (12)		−0.794 (19)		$(\bar{1}\bar{2}7)$
128.8 (16)	27.1 (12)	0.408 (21)		−2.762 (21)	$(1\bar{2}\bar{7})$
	152.9 (12)		0.794 (19)		$(12\bar{7})$
	207.1 (12)	−0.408 (21)			$(\bar{1}2\bar{7})$
	332.9 (12)		−0.794 (19)		$(\bar{1}\bar{2}\bar{7})$
51.2 (16)	62.9 (12)	0.794 (19)	−0.408 (21)	2.762 (21)	$(2\bar{1}7)$
	117.1 (12)		0.408 (21)		(217)
	242.9 (12)	−0.794 (19)			$(\bar{2}17)$
	297.1 (12)		−0.408 (21)		$(\bar{2}\bar{1}7)$
128.8 (16)	62.9 (12)	0.794 (19)		−2.762 (21)	$(2\bar{1}\bar{7})$
	117.1 (12)		0.408 (21)		$(21\bar{7})$
	242.9 (12)	−0.794 (19)			$(\bar{2}1\bar{7})$
	297.1 (12)		−0.408 (21)		$(\bar{2}\bar{1}\bar{7})$

In Figure 2a, the rotation of the unit cell around the zone axis out of the xy plane is graphically demonstrated. The vector of the rotation axis is determined by ψ, which is the

angle between the x axis and the rotation axis, and Φ is the angle between the xy plane and the (001) plane of the rotated unit cell.

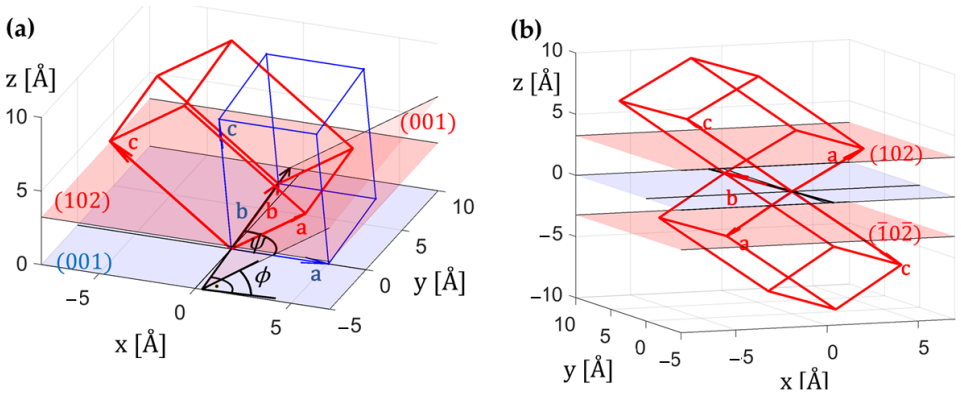


Figure 2. Sketch of the triclinic unit cell of pentacenequinone (P2O) with its lattice vectors **a**, **b,** and **c**. (**a**) The new crystal orientation (colored in red) is obtained by rotation around the axis depicted as black vector. Also shown are the rotation angles ψ and Φ. Blue: unit cell with its contact plane (001), which is identical to the xy plane, also colored in blue. Red: rotated unit cell with its crystallographic planes (001) and (102), which is the contact plane parallel to the xy plane. (**b**) Mirror symmetric unit cells with the contact planes (102) and $(\bar{1}0\bar{2})$.

From Equations (10) and (12), the following relations result, affirming the previously obtained Miller indices of the contact plane (102): v/u = 0.011 and w/u = 1.994. Using Equation (11) and inserting the value of the specular scan (see Table 1), u can be calculated to obtain 1.003. From Equation (14), the alternative orientation parameters u_q, v_q, and w_q were determined (see Table 2).

In our rotating GIXD experiments on epitaxially grown P2O on Ag111, however, unit cells with the contact plane (102) and $(\bar{1}0\bar{2})$ were found [17]. In static GIXD, diffraction peaks from a positive and a negative contact plane cannot be discriminated. Inverting the sign of all Laue indices does not change q_{xyz}, but changes the sign of all Miller indices. The obtained rotation parameters are listed in Table 1. Note that the vector of the rotation axis changes its direction and for the rotation angle, the supplementary angle is obtained, resulting in mirror symmetry. In Figure 2b, the resulting unit cell geometry is graphically sketched.

3.2. Diindenoperylene (DIP) on HOPG—Monoclinic

In Figure 1b, the GIXD pattern of a DIP thin film on HOPG is shown. In total, we used ten Bragg peaks (low mosaicity), based on their q_{xy} and q_z positions, together with the Bragg peak of the specular diffraction pattern (q_{spec}) for our indexing procedure [7]. In this work, we used the previously obtained lattice parameters (see Table 1) and the Laue indices of the ten diffraction peaks. The calculated numbers of the rotation angles Φ and ψ are given in Table 2. In Figure 3a, the resulting geometrical relations are graphically depicted.

From the equations in Appendix C, the following relations result, affirming the previously obtained Miller indices of the contact plane (121): $v/u = \pm 1.981$ and w/u = 0.978. The alternative orientation parameters u_q, v_q, and w_q were determined (see Table 2).

Multiplying u_q, v_q, and w_q with the experimentally obtained length of the specular diffraction peak, one obtains 1.008, ±1.996, and 0.985, respectively.

In monoclinic lattices, the length of the reciprocal vector g_{xyz}, i.e., Equation (2), reduces to the following expression:

$$g_{xyz} = \sqrt{h^2 a^{*2} + k^2 b^{*2} + l^2\, c^{*2} + 2hla^* c^*\, \cos\beta^*}\,. \tag{15}$$

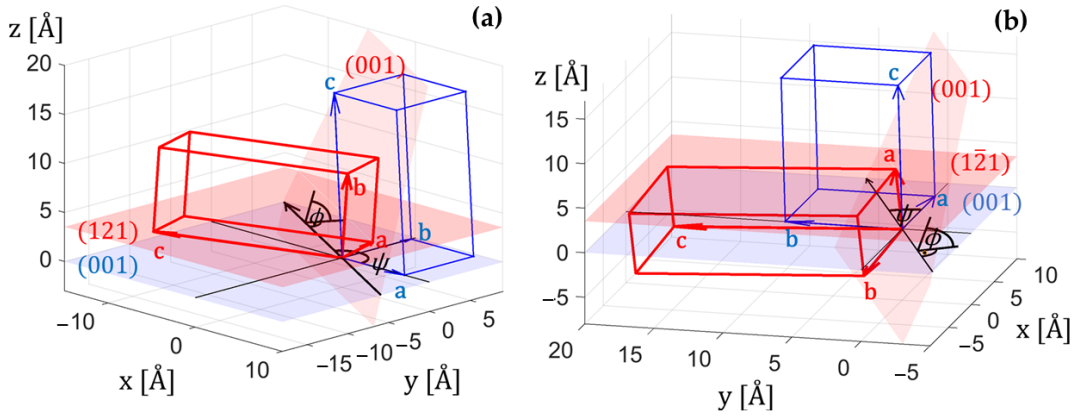


Figure 3. Sketch of the monoclinic unit cell of diindenoperylene (DIP) with its lattice vectors **a**, **b,** and **c**. The new crystal orientation (colored in red) is obtained by rotation around the axis depicted as black vector. Also shown are the rotation angles ψ and Φ. Blue: unit cell with its contact plane (001), which is identical to the *xy* plane, also colored in blue. Red: rotated unit cell with its crystallographic planes (001), (**a**) (121), and (**b**) (1$\bar{2}$1), respectively, parallel to the *xy* plane.

Therefore, inverting the sign of the Laue indices k_i has no effect. The orientation of the unit cell, however, is affected, as the sign of the factor f_2 in Equation (5) must change, i.e., $f_2 \rightarrow -f_2$. Thus, the vector of the rotation axis changes its direction but the rotation angle remains the same. The resulting geometry is graphically shown in Figure 3b; the obtained rotation parameters are listed in Table 2. The resulting contact plane is then $(1\bar{2}1)$. In static GIXD, the diffraction peaks of these two contact planes overlap. The same argument is valid for the contact planes $(\bar{1}2\bar{1})$ and $(\bar{1}2\bar{1})$. The formulae for the rotational parameters in monoclinic systems can be found in Appendix C. In Table 2, the calculated values for the orientation parameters in all four possible cases are listed.

3.3. Binaphthalene on Silicon—Tetragonal

In Figure 1c, the GIXD pattern of binaphthalene (BNP) on silicon is shown. A total of eight reflections of the GIXD map were included in the analysis. Note the significantly reduced texture (high mosaicity) as compared to the previous two examples, which is evident from the Bragg peaks smeared out significantly along common q values resembling Debye Scherrer rings, impeding the assignment of the peak positions associated with their maxima. The lattice parameters were taken from the literature [20] and are listed in Table 1. In a first step, the Laue indices were assigned using the length of the reciprocal vector, g_{xyz}. In tetragonal lattices, the expression for g_{xyz} (*c.f.* Equation (2)) reduces to

$$g_{xyz} = \sqrt{(h^2 + k^2)a^{*2} + l^2\, c^{*2}}\,. \tag{16}$$

Therefore, only the absolute values of the Laue indices can be determined, and the Laue indices h_i and k_i can be interchanged. A further refinement has to be performed using the linear equation for the out-of-plane component g_z (*c.f.* Equation (5)).

In any case, the signs of all groups of Laue indices can be changed, resulting in eight possibilities and, as $a^* = b^*$, a total of 16 possible orientations are obtained. These are listed in Table 2. They result from eight possible orientations of the rotation axis and two rotational angles Φ, which are supplementary. A schematic sketch is shown in Figure 4. Note that in all cases, the interplanar distance between the contact plane and the *xy* plane has the same length ($2\pi/q_{spec}$ = 2.5 Å). In tetragonal systems, as in orthorhombic systems, the derived formulae for the rotational parameters are significantly reduced in complexity; they are given in Appendix C. In Table 2, when determining the ratios w_q/u_q and v_q/u_q,

the values ±6.8 and ±1.9 in the first eight cases and ±3.5 and ±0.5 in the other cases are obtained, respectively. Therefore, the contact planes with the Miller indices $u = \pm 1$, $v = \pm 2$, $w = \pm 7$ and $u = \pm 2$, $v = \pm 1$, and $w = \pm 7$ can be assumed, respectively. From Equation (16), the position of the corresponding specular diffraction peak can be calculated to be 2.52 $Å^{-1}$. Though a specular diffraction experiment was not additionally performed in this study, this peak is present in the powder pattern of the substance.

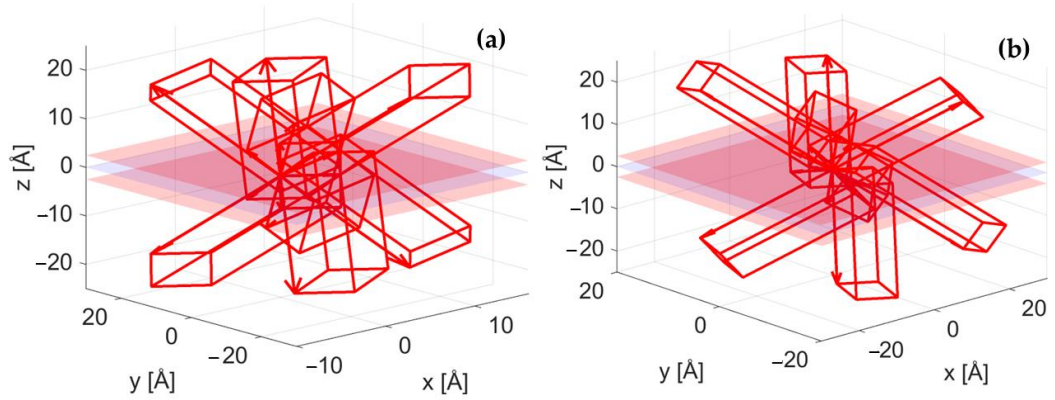


Figure 4. Sketch of the possible orientations of the tetragonal unit cell of binaphthalene (BNP) for (**a**) $u = \pm 1$, $v = \pm 2$, and $w = \pm 7$ and (**b**) $u = \pm 2$, $v = \pm 1$, and $w = \pm 7$. The contact planes (colored in red) are parallel to the xy plane (colored in blue), for $w = 7$ in the positive z direction and for $w = -7$ in the negative z direction. Note that there are no rotational symmetries around the z axis; only mirror symmetries exist.

4. Conclusions

The two-dimensional space maps obtained in static GIXD experiments incorporate the in-plane (q_{xy}) and out-of-plane (q_z) components of the scattering vector. The out-of-plane components are used for determining the crystallographic orientation, which can be characterized either by the rotation angles ψ and Φ or by the Miller indices u, v, and w of its contact (or texture) plane. In the unrotated case, i.e., for the contact plane (001), the unit cell is aligned in the z direction. In the general case, emanating from the (001) plane, by applying a rotation by a specific angle Φ around an axis, whose orientation is characterized by ψ, the contact plane (uvw) can be obtained. Assigning the Laue indices to the diffraction peaks is the prerequisite for determining the orientation of the unit cell. In this work, the mathematical framework that was developed in our previous papers has been extended with respect the orientation parameters. In the equation for q_z, the coefficient associated with the Laue indices l_i contains the information for the rotation angle Φ; the orientation of the rotation axis is incorporated in the other two coefficients. Alternatively, the Miller indices u, v, and w of the contact plane can be chosen as orientation parameters. If the specular diffraction peak q_{spec} is not known, the ratios u_q, v_q, and w_q of the Miller indices with q_{spec} can be used. Equations have been derived to calculate these orientation parameters and the relations between them.

In static GIXD, however, no unique solution for the orientation of the unit cell can be found. The number of possible alignments depends on the crystal system of the unit cell. In triclinic systems, two mirror symmetric geometries of the unit cell exist, as the contact plane can be either (uvw) and –(uvw), corresponding to a change in the direction of the rotation axis and the rotation angles, which are supplementary. In monoclinic systems, if the Miller index v is not zero, four possible orientations exist. In crystallographic systems of higher symmetry possessing contact planes with diverse Miller indices, the situation gets even more complicated due to the multiplicity of planes contributing to the same reflections. In orthorhombic and tetragonal systems, up to eight and sixteen possible orientations can be

found, respectively. This is the consequence of the ambiguity of the Laue indices together with the diversity of the Miller indices of the contact plane.

Author Contributions: Conceptualization, J.S. and R.R.; methodology, J.S.; software, J.S.; validation, J.S., F.G. and R.R.; formal analysis, J.S.; investigation, F.G., S.J. and I.S.; resources, F.G. and S.J.; data curation, F.G.; writing—original draft preparation, J.S.; writing—review and editing, R.R. and I.S.; visualization, J.S. and R.R.; supervision, R.R and I.S.; project administration, R.R. All authors have read and agreed to the published version of the manuscript.

Funding: F.G. acknowledges funding from the Austrian Science Fund (FWF) 10.55776/P34463 and the project NEPHEWS under Grant Agreement No. 101131414 from the EU Framework Program for Research and Innovation Horizon Europe.

Data Availability Statement: The original data presented in the study are openly available in the repository of the TU Graz at https://repository.tugraz.at/uploads/bg1sc-d7d47 (accessed on 4 May 2025).

Acknowledgments: Special thanks to Elettra Sincrotrone Trieste for providing access to the beamline XRD1 (proposal 20240009) and Luisa Barba for her assistance, as well as the DESY synchrotron, where the authors acknowledge experimental support from Wolfgang Caliebe (beamline W1).

Conflicts of Interest: The authors declare no conflicts of interest. The funders had no role in the design of the study; in the collection, analyses, or interpretation of data; in the writing of the manuscript; or in the decision to publish the results.

Abbreviations

The following abbreviations are used in this manuscript:

GIXD	Grazing-incidence X-ray diffraction
P2O	Pentacenequinone
DIP	Diindenoperylene
HOPG	Highly oriented pyrolytic graphite
BNP	Binaphthalene

Appendix A

In the following analysis, a, b, c, α, β, and γ are the parameters of the unit cell in real space, and a^*, b^*, c^*, α^*, β^*, and γ^* are the reciprocal cell parameters [21], which are summarized in Table A1.

Table A1. Relations between the parameters of the reciprocal lattice (a^*, b^*, c^*, α^*, β^*, γ^*) and of the direct lattice (a, b, c, α, β, γ) and the volume of the crystallographic unit cell V.

$a^* = \frac{2\pi bc \sin\alpha}{V}$	$\cos\alpha^* = \frac{\cos\beta\cos\gamma - \cos\alpha}{\sin\beta\sin\gamma}$	$\sin\alpha^* = \frac{V}{abc\sin\beta\sin\gamma}$
$b^* = \frac{2\pi ac \sin\beta}{V}$	$\cos\beta^* = \frac{\cos\alpha\cos\gamma - \cos\beta}{\sin\alpha\sin\gamma}$	$\sin\beta^* = \frac{V}{abc\sin\alpha\sin\gamma}$
$c^* = \frac{2\pi ab \sin\gamma}{V}$	$\cos\gamma^* = \frac{\cos\alpha\cos\beta - \cos\gamma}{\sin\alpha\sin\beta}$	$\sin\gamma^* = \frac{V}{abc\sin\alpha\sin\beta}$
$V = abc\sqrt{1-\cos^2\alpha-\cos^2\beta-\cos^2\gamma+2\cos\alpha\cos\beta\cos\gamma} = abc\sin\alpha^*\sin\beta\sin\gamma$		

If the (001) lattice plane is parallel to the substrate surface, the reciprocal lattice vector $\mathbf{g_{001}}$ with its Laue indices h, k, and l can be represented by the equation

$$\mathbf{g}_{001} = \begin{pmatrix} g_x \\ g_y \\ g_z \end{pmatrix} = \boldsymbol{A}^* \begin{pmatrix} h \\ k \\ l \end{pmatrix}, \tag{A1}$$

where the matrix $\boldsymbol{A}^*$, which contains the reciprocal lattice vectors, is given as

$$\boldsymbol{A}^* = \begin{pmatrix} a^* \sin\beta^* \sin\gamma & 0 & 0 \\ -a^* \sin\beta^* \cos\gamma & b^* \sin\alpha^* & 0 \\ a^* \cos\beta^* & b^* \cos\alpha^* & c^* \end{pmatrix}. \tag{A2}$$

If the substrate normal can be characterized by the Miller indices u, v, and w, the reciprocal lattice vector $\mathbf{g}$ has to be rotated around the zone axis, which is defined by the (001) plane, characterized by its normal vector $\boldsymbol{\sigma_1} = (0, 0, 1)^{\mathrm{T}}$, and the new contact plane (uvw), as characterized by its normal vector $\boldsymbol{\sigma_2} = (u, v, w)^{\mathrm{T}}$. The unit vector $\mathbf{n}$ of the zone axis is calculated by the vector product of $\boldsymbol{\sigma_1}$ and $\boldsymbol{\sigma_2}$, whereas the angle Φ of counterclockwise rotation is obtained by their scalar product. Then, the following expressions can be obtained [6]:

$$\mathbf{n} = \begin{pmatrix} \cos\psi \\ \sin\psi \\ 0 \end{pmatrix}, \tag{A3}$$

and

$$\cos\Phi = \frac{ua^* \cos\beta^* + vb^* \cos\alpha^* + wc^*}{g_{spec}}, \tag{A4}$$

where

$$\cos\psi = \frac{\frac{u}{a}\cos\gamma - \frac{v}{b}}{\sqrt{\left(\frac{u}{a}\right)^2 + \left(\frac{v}{b}\right)^2 - 2\frac{u}{a}\frac{v}{b}\cos\gamma}}, \tag{A5}$$

$$\sin\psi = \frac{\frac{u}{a}\sin\gamma}{\sqrt{\left(\frac{u}{a}\right)^2 + \left(\frac{v}{b}\right)^2 - 2\frac{u}{a}\frac{v}{b}\cos\gamma}}, \tag{A6}$$

and

$$\begin{aligned} g_{spec} = (u^2a^{*2} + v^2b^{*2} + w^2\, c^{*2} + 2uva^*b^* \cos\gamma^* + 2uwa^*c^* \cos\beta^* \\ +2vwb^*c^* \cos\alpha^*). \end{aligned} \tag{A7}$$

In Equation (A7), g_{spec} is the length of the specular diffraction peak. The matrix $\boldsymbol{R}$, which describes a rotation by Φ around the axis $\mathbf{n}$, is given by [22]

$$\boldsymbol{R}(\psi, \Phi) = \begin{pmatrix} \cos^2\psi + \cos\Phi \sin^2\psi & \cos\psi \sin\psi(1 - \cos\Phi) & -\sin\psi \sin\Phi \\ \cos\psi \sin\psi(1 - \cos\Phi) & \sin^2\psi + \cos\Phi \cos^2\psi & \cos\psi \sin\Phi \\ \sin\psi \sin\Phi & -\cos\psi \sin\Phi & \cos\Phi \end{pmatrix}. \tag{A8}$$

In the unrotated case, $\boldsymbol{R}$ is the unit matrix, i.e., if $\Phi = \psi = 0$. Note that a rotation around the z axis can be omitted, as only the in-plane component g_{xy} and the out-of-plane component g_z have to be considered.

Using this rotation matrix, Equation (A1) can be written in two ways

$$\mathbf{g} = \boldsymbol{R}(\psi, \Phi)\boldsymbol{A}^* \begin{pmatrix} h \\ k \\ l \end{pmatrix} = \boldsymbol{R}(u, v, w)\boldsymbol{A}^* \begin{pmatrix} h \\ k \\ l \end{pmatrix}. \tag{A9}$$

From Equations (A5) and (A6), the following expression can be derived:

$$v = u\frac{b}{a}\frac{\sin(\psi - \gamma)}{\sin\psi}. \tag{A10}$$

Appendix B

For n > 3 diffraction peaks, Equation (5) gets overdetermined. Then, it is convenient to use quadratic optimization as follows:

$$\begin{pmatrix} a^{*2}\sum_{i=1}^{N} h_i^2 & a^*b^*\sum_{i=1}^{N} h_ik_i & a^*c^*\sum_{i=1}^{N} h_il_i \\ a^*b^*\sum_{i=1}^{N} h_ik_i & b^{*2}\sum_{i=1}^{N} k_i^2 & b^*c^*\sum_{i=1}^{N} k_il_i \\ a^*c^*\sum_{i=1}^{N} h_il_i & b^*c^*\sum_{i=1}^{N} k_il_i & c^{*2}\sum_{i=1}^{N} l_i^2 \end{pmatrix} \begin{pmatrix} f_1 \\ f_2 \\ f_3 \end{pmatrix} = \begin{pmatrix} a^*\sum_{i=1}^{N} q_{z,i}h_i \\ b^*\sum_{i=1}^{N} q_{z,i}k_i \\ c^*\sum_{i=1}^{N} q_{z,i}l_i \end{pmatrix}, \tag{A11}$$

where $q_{z,i}$ is the out-of-plane component of the ith scattering vector.

Appendix C

From the Equations (A4)–(A6), the following relations between the rotation angles Φ and ψ and the rotation parameters u_q, v_q, and w_q can be derived:

$$\cos\Phi = \frac{u_qa^*\ \cos\beta^* + v_qb^*\cos\alpha^* + w_qc^*}{\sqrt{u_q^2a^{*2} + v_q^2b^{*2} + w_q^2c^{*2} + 2u_qv_qa^*b^*\cos\gamma^* + 2u_qw_qa^*c^*\ \cos\beta^* + 2v_qw_qb^*c^*\cos\alpha^*}}, \tag{A12}$$

$$\cos\psi = \frac{\frac{u_q}{a}\cos\gamma - \frac{v_q}{b}}{\sqrt{\left(\frac{u_q}{a}\right)^2 + \left(\frac{v_q}{b}\right)^2 - 2\frac{u_q}{a}\frac{v_q}{b}\cos\gamma}}, \tag{A13}$$

and

$$\sin\psi = \frac{\frac{u_q}{a}}{\sqrt{\left(\frac{u_q}{a}\right)^2 + \left(\frac{v_q}{b}\right)^2 - 2\frac{u_q}{a}\frac{v_q}{b}\cos\gamma}}. \tag{A14}$$

In monoclinic ($\alpha = \gamma = 90°$) and orthorhombic ($\alpha = \beta = \gamma = 90°$) crystal systems, Equation (14) reduces to the following expressions, respectively:

$$\begin{pmatrix} \frac{2\pi}{a\sin\beta} & 0 & -\frac{2\pi}{c}\cot\beta \\ 0 & \frac{2\pi}{b} & 0 \\ -\frac{2\pi}{a}\cot\beta & 0 & \frac{2\pi}{c\sin\beta} \end{pmatrix} \begin{pmatrix} u_q \\ v_q \\ w_q \end{pmatrix} = \begin{pmatrix} f_1 \\ f_2 \\ f_3 \end{pmatrix}. \tag{A15}$$

Table A2. Expressions for the orientation parameters in monoclinic and orthorhombic crystal systems.

	Monoclinic $\alpha = \gamma = 90°$	Orthorhombic $\alpha = \beta = \gamma = 90°$
$\cos\psi$	$-\frac{f_2}{\sin\Phi}$	
$\tan\psi$	$-\frac{f_1 + f_3\cos\beta}{f_2\sin\beta}$	$-\frac{f_1}{f_2}$
v	$-u\frac{b}{a}\cot\psi$	
w	$u\frac{c}{a}\left[\sin\beta\frac{\cot\Phi}{\sin\psi} + \cos\beta\right]$	$u\frac{c}{a}\frac{\cot\Phi}{\sin\psi}$
$\sin\psi$	$\frac{u_qb}{\sqrt{(u_qb)^2 + (v_qa)^2}}$	
$\cos\psi$	$\frac{-v_qa}{\sqrt{(u_qb)^2 + (v_qa)^2}}$	
$\cos\Phi$	$w_q\frac{2\pi}{c\sin\beta} - u_q\frac{2\pi}{a}\cot\beta$	$w_q\frac{2\pi}{c}$

References

1. Birkholz, M. *Thin Film Analysis by X-Ray Scattering*; Wiley-VCH: Weinheim, Germany, 2006.
2. Witte, G.; Wöll, C. Growth of aromatic molecules on solid substrates for applications in organic electronics. *J. Mater. Res.* **2004**, *19*, 1889–1916. [CrossRef]
3. Tolan, M. *X-Ray Scattering from Soft-Matter Thin Film*; Springer: Berlin/Heidelberg, Germany, 1999.
4. Robinson, I.K.; Tweet, D.J. Surface X-ray diffraction. *Rep. Prog. Phys.* **1992**, *55*, 599–651. [CrossRef]
5. Werzer, O.; Kowarik, S.; Gasser, F.; Jiang, Z.; Strzalka, J.; Nicklin, C.; Resel, R. X-ray diffraction under grazing incidence conditions. *Nat. Rev. Methods Primers* **2024**, *4*, 1–20. [CrossRef]
6. Simbrunner, J.; Simbrunner, C.; Schrode, B.; Röthel, C.; Bedoya-Martinez, N.; Salzmann, I.; Resel, R. Indexing of grazing-incidence X-ray diffraction patterns: The case of fiber-textured thin films. *Acta Cryst.* **2018**, *74*, 373–387. [CrossRef] [PubMed]
7. Simbrunner, J.; Hofer, S.; Schrode, B.; Garmshausen, Y.; Hecht, S.; Resel, R.; Salzmann. Indexing grazing incidence X-ray diffraction patterns of thin films: Lattices of higher symmetry. *J. Appl. Cryst.* **2019**, *52*, 428–439. [CrossRef] [PubMed]
8. Colombi, P.; Zanola, P.; Bontempi, E.; Roberti, R.; Gelfi, M.; Depero, L.E. Glancing-incidence X-ray diffraction for depth profiling of polycrystalline layers. *J. Appl. Cryst.* **2006**, *39*, 176–179. [CrossRef]
9. Breiby, D.W.; Bunk, O.; Andreasen, J.W.; Lemke, H.T.; Nielsen, M.M. Simulating X-ray diffraction of textured films. *J. Appl. Cryst.* **2008**, *41*, 262–271. [CrossRef]
10. Krauss, T.N.; Barrena, E.; Zhang, X.N.; de Oteyza, D.G.; Major, J.; Dehm, V.; Würthner, F.; Cavalcanti, L.P.; Dosch, H. Three-Dimensional Molecular Packing of Thin Organic Films of PTCDI-C8 Determined by Surface X-ray Diffraction. *Langmuir* **2008**, *24*, 12742–12744. [CrossRef] [PubMed]
11. Baker, J.L.; Jimison, L.H.; Mannsfeld, S.; Volkman, S.; Yin, S.; Subramanian, A.S.; Alivisatos, A.P.; Toney, M.F. Quantification of thin film cristallographic orientation using X-ray diffraction with an area detector. *Langmuir* **2010**, *26*, 9146–9151. [CrossRef] [PubMed]
12. Mannsfeld, S.C.B.; Tang, M.L.; Bao, Z. Thin Film Structure of Triisopropylsilylethynyl-Functionalized Pentacene and Tetraceno[2,3-b]thiophene from Grazing Incidence X-Ray Diffraction. *Adv. Mater.* **2011**, *23*, 127–131. [CrossRef] [PubMed]
13. Smilgies, D.-M. Grazing-incidence X-ray scattering of lamellar thin films. *J. Appl. Cryst.* **2019**, *52*, 247–251. [CrossRef]
14. Khalil, I.E.; Fonseca, J.; Reithofer, M.R.; Eder, T.; Chin, J.M. Tackling orientation of metal-organic frameworks (MOFs): The quest to enhance MOF performance. *Coord. Chem. Rev.* **2023**, *481*, 215043. [CrossRef]
15. Gasser, F.; John, S.; Smets, J.; Simbrunner, J.; Fratschko, M.; Rubio-Giménez, V.; Ameloot, R.; Steinrück, H.-G.; Resel, R. A systematic approach for quantitative orientation and phase fraction analysis of thin films through grazing incidence X-ray diffraction. *arXiv* **2025**, arXiv:2503.20625.
16. Simbrunner, J.; Salzmann, I.; Resel, R. Indexing of grazing-incidence X-ray diffraction patterns. *Crystallogr. Rev.* **2023**, *29*, 19–37. [CrossRef]
17. Simbrunner, J.; Schrode, B.; Domke, J.; Fritz, T.; Salzmann, I.; Resel, R. An efficient method for indexing grazing-incidence X-ray diffraction data of epitaxially grown thin films. *Acta Cryst.* **2020**, *76*, 345–357. [CrossRef] [PubMed]
18. Simbrunner, J.; Schrode, B.; Hofer, S.; Domke, J.; Fritz, T.; Forker, R.; Resel, R. Searching for New Polymorphs by Epitaxial Growth. *J. Phys. Chem. C* **2021**, *125*, 618–626. [CrossRef] [PubMed]
19. Kainz, M.P.; Legenstein, L.; Holzer, V.; Hofer, S.; Kaltenegger, M.; Resel, R.; Simbrunner, J. GIDInd: An automated indexing software for grazing-incidence X-ray diffraction data. *J. Appl. Cryst.* **2021**, *54*, 1256–1267. [CrossRef] [PubMed]
20. Kress, R.B.; Duesler, E.N.; Etter, M.C.; Paul, I.C.; Curtin, D.Y. Solid-state resolution of binaphthyl: Crystal and molecular structures of the chiral (A)1 form and racemic (B)1 form and the study of the rearrangement of single crystals. Requirements for development of hemihedral faces for enantiomer identification. *J. Am. Chem. Soc.* **1980**, *102*, 7709–7714. [CrossRef]
21. Shmueli, U. *Theories and Techniques of Crystal Structure Determination*; Oxford University Press: Oxford, UK, 2007.
22. Shmueli, U. (Ed.) *Vol. B of International Tables for Crystallography*, 2nd ed.; Springer: Berlin/Heidelberg, Germany, 2006.

Disclaimer/Publisher's Note: The statements, opinions and data contained in all publications are solely those of the individual author(s) and contributor(s) and not of MDPI and/or the editor(s). MDPI and/or the editor(s) disclaim responsibility for any injury to people or property resulting from any ideas, methods, instructions or products referred to in the content.